

Harmonia: Algorithm-Hardware Co-Design for Memory- and Compute-Efficient BFP-based LLM Inference

Xinyu Wang¹, Jieyu Li², Yanan Sun¹, and Weifeng He^{1,*}

¹Shanghai Jiao Tong University, ²Columbia University
 {xinyu2001, sunyanan, hewf}@sjtu.edu.cn, jl7402@columbia.edu

Abstract—Large Language Models (LLMs) are powerful but costly to run in terms of memory and compute. Quantization is particularly effective since it reduces both model size and compute cost. A widely adopted configuration uses integer (INT) weights with floating-point (FP) activations to preserve accuracy. To further reduce the overhead of FP arithmetic, prior works convert FP activations in linear layers into block floating point (BFP), where a group of activations shares a single exponent. However, prior works failed to extend BFP to attention layers due to significant accuracy loss, leading to suboptimal efficiency.

To address this issue, we propose Harmonia, an algorithm-hardware co-design framework that supports an all-layer BFP format and integrates a configurable hardware design. First, to enable all-layer BFP-activations, we systematically explore BFP configurations to achieve a better trade-off between model accuracy and activation compression. Second, to further reduce KV-cache related storage and computation in attention layers, we propose an asymmetric bit-allocation strategy, combined with a hybrid offline-online outlier smoothing technique. Based on this, we aggressively compress the KV-cache from FP16 to 4b-mantissa BFP, with an average loss of only 0.3%. Third, to fully exploit the benefits of all-layer BFP-activations, we propose a suite of dedicated hardware designs for Harmonia. Specifically, we propose a reconfigurable PE unit supporting mixed data formats (i.e., BFP-INT, BFP-BFP) and mixed data precisions, a real-time FP16-to-BFP converter for on-the-fly activation compression, and a flexible tiling-aware dataflow to reduce external memory traffic. We evaluate Harmonia on general matrix multiplication (GEMM) in both linear layers and attention layers across eight widely used LLMs. Compared with prior works, experimental results show that Harmonia achieves 3.84 \times (up to 5.05 \times) higher area efficiency, 2.03 \times (up to 3.90 \times) better energy efficiency, and 3.08 \times (up to 4.62 \times) speedup on average, respectively.

I. INTRODUCTION

Large Language Models (LLMs) [59], [60], [26], [68], [1], [51], [10] have emerged as a transformative foundation in artificial intelligence, demonstrating remarkable proficiency across a wide range of natural language processing tasks, including recommendation systems, chatbots, and personal agents. Guided by the scaling law [32], the most advanced LLMs' parameters have grown to hundreds of billions, posing substantial demands on both memory and computational resources. For instance, deploying a Llama-3.1-405B model, which occupies around 800GB of memory, requires at least 10 high-end H100 GPUs. Additionally, during the generation phase, the auto-regressive nature of LLMs necessitates

recurrent retrieval of a large number of previously generated tokens, resulting in a memory bandwidth bottleneck [37], [2], [34], [56], which severely impacts the performance and efficiency of model inference. These challenges emphasize an urgent need to improve the efficiency of LLM deployment.

Quantization is an effective approach for efficient model deployment. [72], [63], [3], [65], [41], [44], [58] quantize both floating-point (FP) weights and FP activations to low-precision integers. While weights can be statically quantized offline after training, the dynamic nature of activations necessitates runtime quantization, introducing additional latency and hardware costs [24], [36], [69], [33]. As a practical alternative, the weight-only quantization scheme [17], [13], [62], [40], [47], [11], [35], [12], [53] where only weights are quantized to low bits (e.g., INT4), while activations remain in FP format (e.g., FP16), has been widely adopted. It can effectively reduce the model size while preserving the model's linguistic capabilities. However, this scheme still involves costly FP-related operations (e.g., exponent alignment and normalization) and FP-format storage [25], leading to significant hardware overhead.

To alleviate this issue, FIGNA [25] and Anda [16] propose to convert FP activations into the block floating point (BFP) format, where all elements within a block share a common exponent. This shared-exponent feature eliminates the need for costly per-element exponent alignment and normalization, enabling more efficient BFP-related multiplication and accumulation (MAC) on hardware.

However, these designs have two major limitations. First, they fail to extend the BFP format to FP activations in attention layers, which constitute a critical component of LLM architectures. As shown in Fig. 1(a), the dominant computation shifts between linear and attention layers depending on the input sequence length and model configuration. In short-context scenarios [6], [38], linear layers prevail across models of different scales, whereas in long-context applications [4], [70], [29], attention layers rapidly become the primary computational bottleneck as sequence length increases. Consequently, optimizing both layers is equally critical to achieving efficient and flexible adaptation across diverse workloads. Since both designs leave attention activations to be processed by conventional FP-based units, the computation

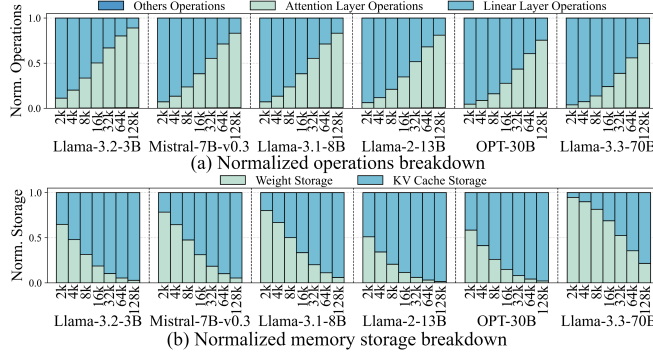


Fig. 1. Normalized breakdown of (a) operations and (b) memory storage for models of different scales under varying sequence lengths.

cost still leaves substantial room for improvement.

Second, both designs retain the Key-Value (KV) cache in FP16 format, overlooking the frequent external memory accesses (EMA) it incurs. The KV cache stores intermediate attention keys and values, and can occupy over 90% of the total memory footprint when the sequence is sufficiently long [34]. As shown in Fig. 1(b), its size scales linearly with sequence length, resulting in substantial EMA overhead. This excessive traffic becomes a major bottleneck during the decoding stage [23], [37], [22], where computation is largely memory-bound and inference throughput is severely constrained. Therefore, maintaining the KV cache in full precision yields no tangible benefit in reducing EMA power or bandwidth pressure.

To overcome these limitations, we propose **Harmonia**, an algorithm-hardware co-design framework that incorporates a unified BFP representation across activations in both linear and attention layers, supported by a configurable compute core capable of executing both BFP-INT and BFP-BFP operations. We begin by empirically exploring the feasibility of extending the BFP format to all-layer activations. Through experiments, we identify a BFP configuration that balances model accuracy and activation compression. Building upon this basis, we further propose an asymmetric bit-allocation strategy and a hybrid offline-online outlier smoothing technique to compress the KV cache from FP16 to 4-bit mantissas without noticeable accuracy loss (only 0.3% on average).

To fully leverage the benefits of the all-layer BFP-based activation representation, **Harmonia** integrates a suite of dedicated hardware units, including a reconfigurable PE unit for mixed data formats and precisions, a real-time FP16-to-BFP converter for on-the-fly activation compression, and a flexible tiling-aware dataflow to reduce the cost of EMA. Through these co-design approaches, **Harmonia** achieves a balanced trade-off among model accuracy, energy consumption, and computational efficiency.

In summary, our contributions are as follows:

- We extend the BFP format to all activations in linear and attention layers, adopting a well-selected configuration with a group size of 32 and 8-bit mantissas for all activations except the KV cache.
- We propose an asymmetric bit allocation strategy and an offline-online hybrid outlier smoothing technique that

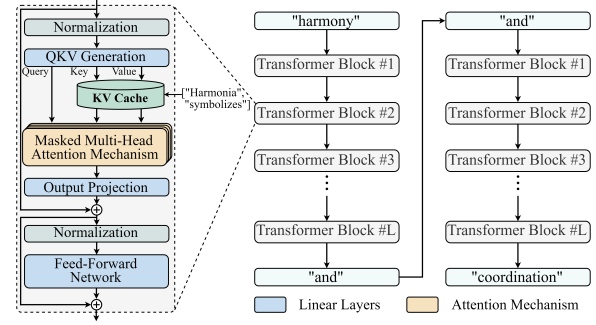


Fig. 2. Illustration of auto-regressive LLM architecture.

together compress the KV cache to 31.25% of its original size with negligible accuracy loss.

- We design a reconfigurable PE unit that unifies BFP-INT and BFP-BFP operations, achieving up to 4.85 \times higher area efficiency and 4.52 \times better energy efficiency over baselines.
- Based on the above techniques, we present **Harmonia**, an LLM accelerator that dynamically compresses activations and supports flexible arithmetic across heterogeneous precisions and formats. Compared with SOTA accelerators, **Harmonia** achieves up to 5.05 \times higher area efficiency, 3.90 \times higher energy efficiency, and 4.62 \times speedup, with average gains of 3.84 \times , 2.03 \times , and 3.08 \times , respectively.

II. BACKGROUND AND MOTIVATION

This section first outlines the LLM inference process, then introduces the existing quantization techniques. After that, we further analyze the limitations of existing methods, which reveal opportunities and motivate our design.

A. LLM Inference Process

As shown in Fig. 2, LLMs are built upon the Transformer architecture [61], which stacks multiple Transformer blocks composed of several linear layers and a masked self-attention mechanism. The generative inference of LLMs consists of two stages: prefilling and decoding. In the prefill stage, the prompt tokens are first processed through three linear layers to produce the Query (Q), Key (K) and Value (V) matrices. The attention scores are then derived from Q and K, which are subsequently used to perform a weighted sum over the V matrix. The intermediate results generated by the attention block are then passed through a feed-forward network to produce the final output. Meanwhile, the K and V matrices produced in this stage are stored as the KV cache, which serves to avoid redundant computation in the subsequent decode stage. During decoding, the newly generated token, together with the cached K and V, is used to generate the next token and update the KV cache repeatedly until a termination condition is met.

In terms of computation, both linear and attention layers in LLMs are fundamentally composed of GEMM in the prefill stage and GEMV in the decode stage. Supposing the hidden dimension of the model is d , the lengths of the input prompt and the generated tokens are n and l separately, the operations in linear layers scale with $(n+l)d^2$, whereas those in attention

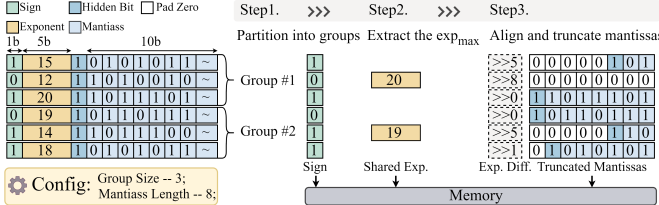


Fig. 3. Illustration of the FP16-to-BFP conversion with a group size of 3 and an 8-bit mantissa.

layers scale with $d(n^2 + \frac{1}{2}l^2 + (n-1)l)$. Importantly, since the sequence length in real-world LLM applications varies from thousands to millions [14], [5], while d remains constant after training, the computational bottleneck shifts between linear and attention layers depending on the workload. In terms of memory, the footprint is dominated by two major components: weights and the KV cache, either of which can become the limiting factor under different scenarios [56], [37].

Therefore, alleviating the computational overhead in both linear and attention layers, as well as reducing accesses to weights and the KV cache stored in external memory, is critical to improving inference efficiency.

B. Quantization Techniques

Quantization is an effective technique that converts high-precision values to low-bit formats, reducing computation and memory costs. In particular, quantizing weights to integer formats offline has been shown to be highly effective. However, activation quantization is more challenging due to its wider value distributions and the presence of outliers, which can severely degrade accuracy. Moreover, it requires dynamically computing scaling factors and offsets to adapt to the runtime value variations. This introduces additional hardware into existing pipelines [24] and sometimes requires system-level support [43], [72] to fully unlock its benefits.

While the INT-weight and FP-activation scheme can greatly reduce the memory cost for LLM inference, it cannot avoid expensive FP-based MAC operations, which require exponent alignment and normalization. To mitigate this issue, recent works convert FP activations in linear layers to the BFP format, which shares the same exponent within a group. It achieves a balance between the dynamic range of FP formats and the simplicity of INT-based MAC operations.

Fig. 3 shows the steps to convert an FP16 vector to BFP: (1) partition the vector into groups, (2) extract the largest exponent in each group as the shared exponent, and (3) right-shift and truncate mantissas based on exponent differences. Evidently, the group size and mantissa precision directly determine the numerical error introduced by this process. In general, smaller groups with sufficient mantissa bits yield lower error, while larger groups and aggressive truncation increase the error, which can degrade model accuracy. Thus, selecting an appropriate BFP configuration to balance model accuracy and efficiency remains a non-trivial challenge.

To mitigate the impact of numerical errors on model accuracy, one feasible strategy is BFP-aware training [67], [9], [50], [18], which directly adopts the BFP format during

training. However, LLM training is prohibitively expensive [8], [21], [28], [60], requiring massive computation and time, which limits its practicality. Instead, another line of work introduces BFP conversion at inference time. FIGNA [25] adopts a conservative strategy by analytically relating mantissa bit width to numerical precision and extending the mantissa to match FP-based results. Although this preserves accuracy, storing activations in FP16 format eliminates both memory and bandwidth savings. Anda [16] employs a customized search algorithm to allocate variable mantissa bit widths to different types of activations in linear layers under bounded accuracy loss, aiming to minimize total bit operations.

However, prior efforts mainly target linear layers, neglecting FP-FP operations between activations in attention layers and the substantial storage overhead of the KV cache. To fully exploit the potential of the BFP format, it is essential to explore the feasibility of converting all activations involved in LLM inference into the BFP format and, on this basis, aggressively compress the KV cache to minimize storage cost.

C. Opportunities and Challenges

In this work, we investigate the possibility of converting all FP16 activations into the BFP format, including those involved in linear layers as well as the Q, K, V representations and attention scores within the attention mechanism. To assess the impact of different BFP configurations on model accuracy, we adopt perplexity on the WikiText2 dataset [48] as the evaluation metric and evaluate eight widely used pre-trained models as benchmarks. The perplexity of the full-precision model serves as the 100% baseline, and the relative performance across various mantissa bit widths and group sizes is shown in Fig. 4.

The results indicate that model accuracy is highly sensitive to the mantissa bit width. Each subplot of Fig. 4 demonstrates that different models exhibit varying levels of accuracy degradation under the same BFP configuration, but they share a consistent trend: accuracy decreases as the mantissa bit width shrinks. Notably, when the bit width drops below 8 bits, accuracy declines sharply. Using 8-bit mantissas keeps the accuracy degradation around 1.5% for most models, which we consider an acceptable loss. Therefore, all subsequent analyses and experiments adopt 8-bit mantissas for activations except those in the KV cache.

Furthermore, by comparing different subplots in Fig. 4, we observe that the group size also plays a crucial role in determining model accuracy. Larger groups achieve a higher activation compression rate but amplify accuracy loss caused by truncated mantissas. To balance accuracy and memory efficiency, we adopt a group size of 32 for all activations under the 8-bit mantissa configuration.

To further mitigate the memory overhead of the KV cache, we evaluate the impact of truncating its mantissas to lower bit widths. In this experiment, the group size is fixed at 32, and the mantissa length of other activations is set to 8. We then gradually reduce the KV cache mantissa precision from 8 to 1 bit to evaluate accuracy degradation with decreasing bit width.

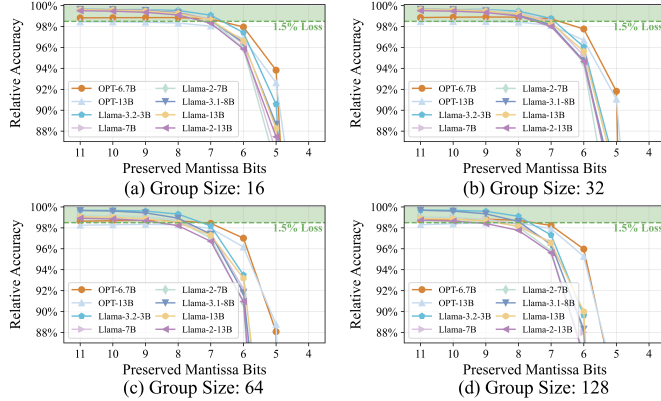


Fig. 4. Relative accuracy of different models under various preserved mantissa bits and group sizes.

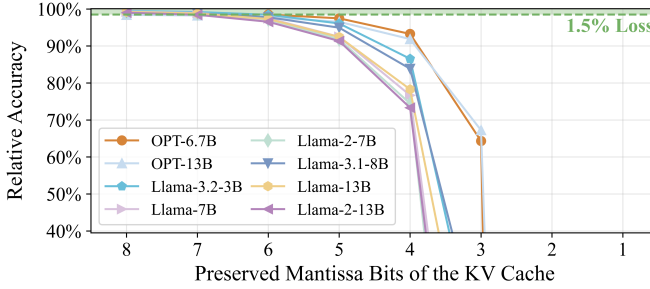


Fig. 5. Relative accuracy of different models under various preserved mantissa bits of the KV cache.

As shown in Fig. 5, accuracy deteriorates progressively with aggressive truncation and drops sharply below 5 bits. For most models, the relative accuracy falls below 90%, and in some cases approaches 70% at 4 bits. These results highlight the challenge of compressing the KV cache to ultra-low bit widths while maintaining acceptable accuracy, motivating the need for advanced strategies to balance precision and efficiency.

In summary, our study reveals two key insights. **First (Opportunity)**, with a well-chosen combination of group size and mantissa length, model accuracy can be maintained within an acceptable margin. **Second (Challenge)**, compressing the KV cache to ultra-low bits remains difficult and causes severe accuracy loss, hindering practical deployment. These findings motivate us to extend the BFP format to all activations in LLMs to fully exploit its potential. In addition, it highlights the need for advanced optimization strategies to mitigate the accuracy loss incurred by aggressive KV-cache compression.

III. HARMONIA ALGORITHM

This section presents the algorithmic foundation of Harmonia. Based on the experimental results in Sec. II-C, we set the group size to 32, adopt a 5-bit shared exponent per group, and use an 8-bit mantissa for activations except the KV cache. In this section, we begin by introducing a dynamic BFP conversion framework, which converts activations to the BFP format during inference. To mitigate the accuracy loss caused by compressing the KV cache to 4-bit mantissas, we propose two key optimizations: (1) an initial-local asymmetric bit allocation strategy and (2) an offline–online hybrid outlier smoothing technique. Finally, we analyze the hardware

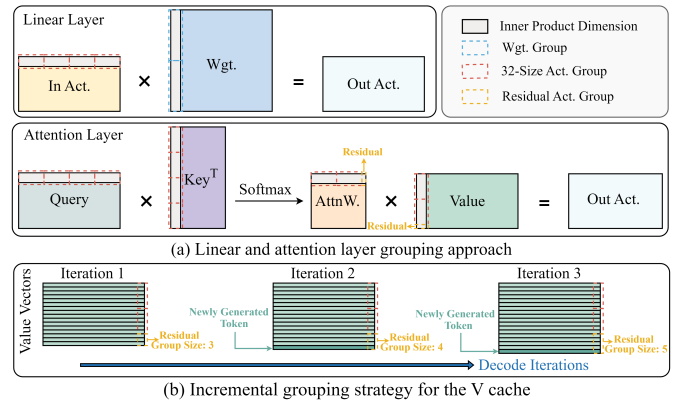


Fig. 6. (a) Grouping strategies for different activation types. (b) Incremental grouping strategy applied to the V cache.

benefits of BFP-based conversion, which motivate the unified and efficient architecture of Harmonia.

A. BFP Conversion Framework

Given the dynamic nature of activations, online conversion to the BFP format at runtime is essential. To fully exploit BFP’s shared-exponent property, activation grouping must align with the inner-product computation direction. As shown in Fig. 6(a), activations in both linear and attention layers are grouped per token, except for the Value (V) matrix. This grouping strategy aligns well with the streaming pattern of the inference process, because the hidden dimension is an integer multiple of the group size in both the prefill and decode stages.

In contrast, for V, the dynamic growth of the sequence length disrupts group completeness, meaning that the most recent tokens may not form a full group. We refer to this partial block as a residual group. To address this issue, we propose an incremental grouping strategy for BFP conversion of V, as illustrated in Fig. 6(b). Instead of waiting for a full group to form, each newly generated token is iteratively appended to the residual group, which is temporarily converted based on its current size to produce intermediate results. The residual group is updated at every iteration as a new token arrives. Once the group reaches the predefined size, a final BFP conversion is performed, and the result is committed to the V cache.

This strategy ensures that all MACs are performed using BFP-formatted activations, thereby avoiding the requirement to introduce additional hardware units dedicated to handling the V vectors in the residual group and streamlining the overall datapath for a more compact and efficient design.

B. Initial-Local Asymmetric Bit Allocation

To address the challenge outlined in Sec. II-C of recovering model accuracy when truncating the KV cache mantissas to extremely low bit widths, we begin by analyzing the attention score distributions across different models. As illustrated in Fig. 7, this analysis reveals an important phenomenon: the model exhibits a strong tendency to focus on the initial few tokens and the most recent tokens, indicating a clear temporal pattern in the attention distribution. This observation reveals that model accuracy is particularly sensitive to the precision

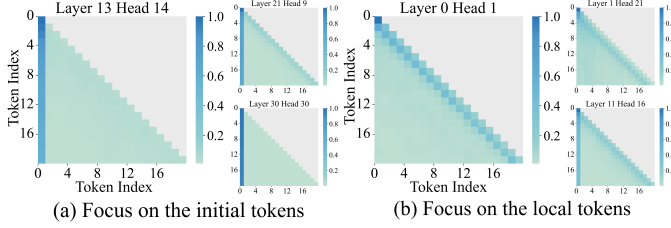


Fig. 7. Average attention scores in Llama-3.1-8B over 128 sentences, each with a length of 20: (a) initial-token attentive heads, (b) local-token attentive heads.

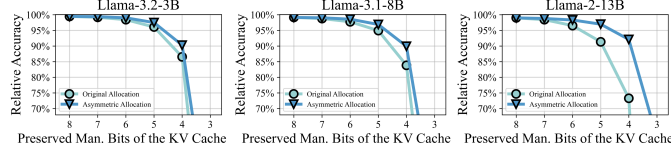


Fig. 8. Accuracy improvement across three models achieved by applying the asymmetric bit-allocation strategy.

of these initial and local tokens, as they play a pivotal role in guiding the generation process.

Motivated by this insight, we propose an asymmetric bit allocation strategy that adaptively assigns higher precision to these critical regions of the sequence. Specifically, the mantissas of the initial and local tokens in the KV cache are allocated 8-bit precision, while those of others are truncated to 4 bits. The numbers of the initial and local tokens are 32 and 64, respectively. Under a 4K sequence length, 97.6% of the KV cache adopts a 4-bit mantissa while only 2.4% uses an 8-bit mantissa, reducing the KV-cache storage by 3.05 \times .

To validate the effectiveness of this strategy, Fig. 8 compares three representative models with and without the asymmetric bit allocation. As shown in the figure, our approach achieves notable accuracy improvements, with a relative accuracy gain of 9.54% across three models on average, effectively mitigating the precision loss caused by low-bit mantissas of the KV cache. The results show that this strategy preserves the attention fidelity of contextually important tokens while substantially reducing computation and memory overhead, achieving a favorable balance between accuracy and efficiency.

C. Offline-Online Hybrid Outlier Smoothing

Although our asymmetric bit-allocation strategy can improve the accuracy, it still poses notable accuracy loss compared to the BFP with the 8b-mantissa scheme. We have found that this is because of the presence of outliers. We analyze the magnitude distribution of KV cache values in Fig. 9. The V matrix exhibits a relatively uniform distribution, while K shows clear channel-wise outliers. When K is grouped across channels (i.e., along the token dimension) for BFP conversion under our grouping strategy, these outliers dominate the shared exponent, forcing smaller values to zero. The resulting conversion errors propagate through the attention scores and further to the outputs, ultimately degrading accuracy. To mitigate this, we propose an offline-online hybrid outlier smoothing technique that suppresses such outliers. After outlier smoothing, the magnitude distribution will be more concentrated, which makes it easier to realize the 4-b

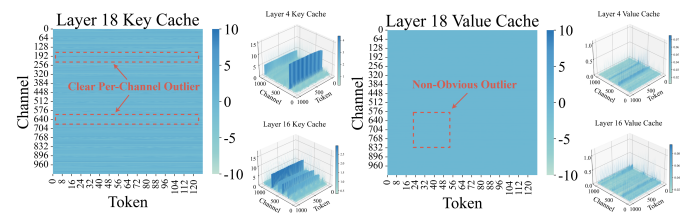


Fig. 9. Magnitude distribution of values in the KV cache of Llama-3.1-8B. mantissa truncation without large accuracy loss.

For offline smoothing, we introduce a per-channel scaling mechanism to smooth outliers in K. We define a scaling factor $S \in \mathbb{R}^{1 \times C}$, where C denotes the hidden dimension of K. Each channel of K is multiplied by its corresponding scaling factor s_c , while the corresponding channel of Q is divided by s_c to preserve the original results, which can be described as:

$$P = \text{softmax}(QK^T) = \text{softmax}((Q \oslash S) \cdot (K^T \odot S)) \quad (1)$$

To implement this offline smoothing, there are two key challenges. First, dynamically applying per-channel scaling to Q and K during inference complicates the datapath and increases the computation overhead at runtime. Second, determining appropriate scaling factors remains non-trivial. To address the first issue, we observe that the Q and K are derived from the input activations through linear projections. This provides an opportunity to absorb the scaling factors into the weights of linear layers, thereby eliminating the need for explicit scaling during inference. Under this transformation, Eq. (1) can be reformulated as:

$$P = \text{softmax}((X \cdot (W_Q \oslash S)) \cdot ((W_K^T \odot S) \cdot X^T)) \quad (2)$$

To address the second issue, different from activation-aware weight quantization approaches, such as SmoothQuant [63] and AWQ [42], which hand-craft the scaling factors, we treat the scaling factors as learnable parameters. This allows the scaling to be adaptively optimized, enabling a better match to the characteristics of different models. Specifically, we employ a calibration dataset to determine the optimal S that minimizes the mean square error (MSE) between the original block outputs and the outputs produced when applying the scaling to Q and K. The optimization objective can be formulated as:

$$S = \arg \min_S \|\mathcal{F}(W, X) - \mathcal{F}(W, \text{Convert}_{\text{BFP}}(X); S)\|_2^2 \quad (3)$$

where \mathcal{F} represents a transformer block function, W and X are full precision weights and activations, $\text{Convert}_{\text{BFP}}$ represents the BFP converter, and S is a learnable vector of scaling factors. As illustrated in Fig. 10, after applying our scaling-based smoothing strategy, the channel-wise outliers are effectively suppressed, and the overall distribution of K becomes more uniform, indicating improved numerical stability for subsequent BFP conversion.

Notably, the results in Fig. 10 also highlight an additional opportunity for improvement: while outliers are suppressed, the values in previously non-outlier channels are amplified, leading to a wider overall value range and introducing potential

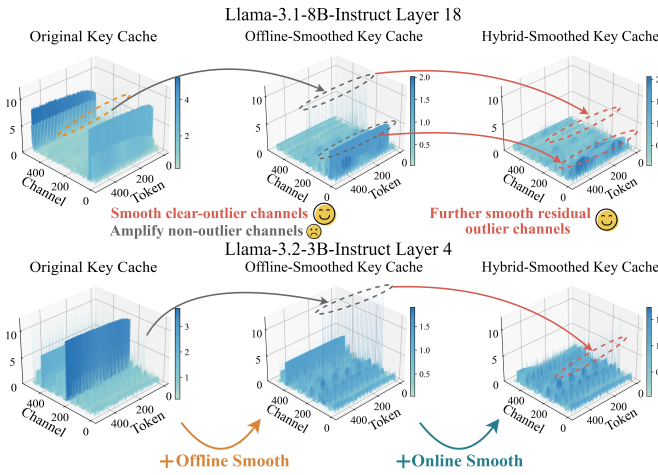


Fig. 10. Effect of outlier suppression using the offline-online hybrid smoothing strategy.

numerical instability. To mitigate this, we apply the online smoothing, i.e., an incremental optimization that adaptively handles dynamically changing distributions during inference. As shown in Fig. 9, K exhibits a clear intra-channel similarity across tokens. Additionally, because of the shift-invariance property of the softmax operation, subtracting a per-channel offset from K does not affect the resulting attention scores. Leveraging these two properties, we perform online smoothing on a subset of K channels with prominent outliers to stabilize their value ranges. To minimize runtime overhead, we adopt a lightweight offset selection strategy. Specifically, we first identify the maximum absolute value for each channel within the initial 32-token window. Then, we select the top- k channels with the largest magnitudes and assign half of each as the corresponding channel offset, while setting the offset of the remaining channels to zero. As illustrated in Fig. 10, applying online smoothing effectively suppresses outlier-induced divergence.

In summary, the proposed offline-online hybrid smoothing effectively suppresses outliers, achieving a balance between numerical stability and low runtime hardware overhead. This approach lays a solid foundation for simple and efficient hardware implementations in large-scale LLM inference.

D. Unified Integer-based BFP-INT and BFP-BFP MACs

Building on the above algorithmic optimizations, we enable the conversion of activations in both linear and attention layers to the BFP format during inference. This transformation lays the groundwork for a unified hardware execution of BFP-INT and BFP-BFP MACs on a single compute core. In conventional FP-based inner-product computation, partial products carry different exponents, requiring dynamic alignment through a costly arbitrary-bit barrel shifter in each PE. In contrast, the BFP format enforces a shared exponent within each group, allowing direct integer accumulation without per-element alignment. The accumulated result is then normalized once per group, amortizing the normalization overhead. This numerical format conversion simplifies the datapath and enhances computational efficiency.

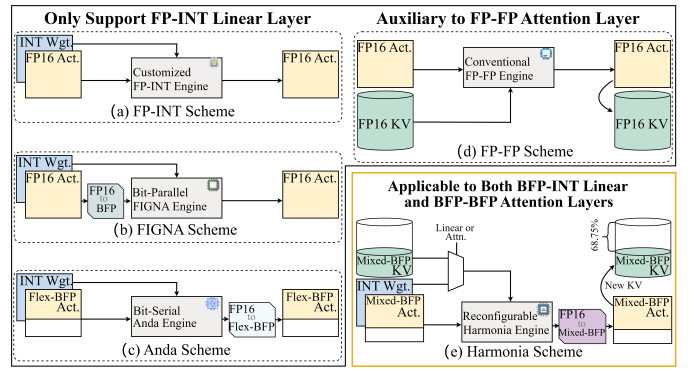


Fig. 11. Comparison of different compute schemes: (a) customized FP-INT scheme, (b) FIGNA scheme, (c) Anda scheme, (d) conventional FP-FP scheme, and (e) the proposed Harmania scheme.

To intuitively demonstrate the hardware benefits introduced by Harmania’s algorithms, Fig. 11 illustrates the computation flows of the linear and attention layers across four representative designs. Fig. 11(a) shows that the dedicated FP-INT engine removes the FP dequantization step required in GPUs but still suffers from costly alignment and normalization inherent in FP-based calculation. As shown in Fig. 11(b) and (c), both FIGNA [25] and Anda [16] employ FP-to-BFP conversion to perform integer-based MACs. FIGNA retains FP16 activations and converts them to extended-mantissa BFPs before computation, incurring extra access and conversion overhead without reducing memory cost. Anda stores activations in variable mantissa bit widths to cut memory traffic, but its bit-serial design adds timing and hardware complexity. However, all three designs still rely on an additional FP-FP engine shown in Fig. 11(d) for attention layers, diminishing overall performance gains when attention layers dominate computational workload in long-context scenarios.

Fig. 11(e) illustrates the key advantages of Harmania over prior designs. First, both linear and attention operations can be executed on a single reconfigurable core (detailed in Sec. IV), enabling efficient resource sharing and high hardware utilization. Second, truncated-mantissa BFP representation of activations lowers storage overhead. Finally, to mitigate the KV cache growth during generation, Harmania compresses it to 31.25% of its original size, substantially reducing storage footprint and memory access overhead.

IV. HARMONIA ARCHITECTURE

This section presents the Harmania architecture, designed to accelerate operations in both linear and attention layers. We first outline the overall Harmania system, then detail its three key components: (1) a reconfigurable PE that supports MACs across heterogeneous data precisions and formats, (2) a real-time BFP converter for on-the-fly activation conversion, and (3) a tiling-aware dataflow that optimizes memory access.

A. Overview

Fig. 12 illustrates the overall Harmania architecture, which integrates a reconfigurable PE array, a real-time BFP converter, a dataflow controller, an online channel-wise K-offset generator, high-density dual-port on-chip SRAMs,

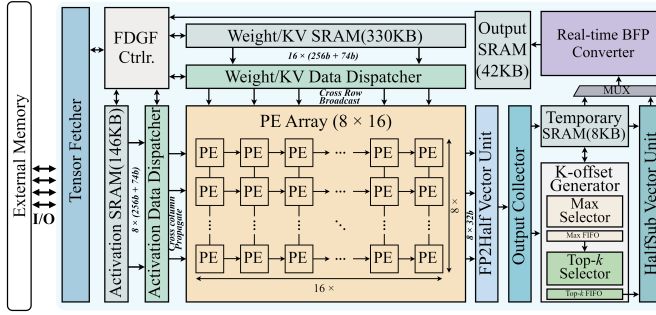


Fig. 12. The overall architecture of Harmonia.

data dispatchers, and vector units. During runtime, the computation proceeds as follows:

(1) The controller instructs the tensor fetcher to load INT4 weights and BFP-formatted activations from external memory into on-chip SRAMs. (2) Once ready, the weight and activation dispatchers stream data to the PE array under the controller’s coordination. To maximize data reuse, weights are broadcast across rows, while activations propagate across columns in a systolic pattern. (3) The 8×16 PE array then performs BFP-INT or BFP-BFP MACs, depending on input precision and type, following an output-stationary dataflow. Accumulation results are stored in FP32 format to maintain numerical accuracy. (4) After computation, the FP2Half vector unit converts outputs to FP16 format and stores them in the temporary SRAM. (5) For K-type activations in the initial window (detailed in Sec. III-B), they are forwarded to the online K-offset generator to produce per-channel offsets. For others, this path is bypassed, and this unit is clock-gated to save power. (6) When valid results are available, the BFP converter performs online FP16-to-BFP conversion. (7) Finally, the controller transfers the converted results back to external memory for subsequent operations.

B. Reconfigurable PE Unit

To translate algorithmic optimizations into hardware efficiency, we design a reconfigurable PE unit that flexibly supports mixed-precision and heterogeneous-format computation, as illustrated in Fig. 13. It supports three distinct computation modes: (1) M8W4, which performs MACs between 8-bit-mantissa activations and INT4 weights, (2) M8M4, which performs MACs between activations with 8-bit and 4-bit mantissas, and (3) M8M8, which performs MACs between activations with 8-bit and 8-bit mantissas. The first mode is applied to linear layers, while the latter two are used in attention layers to accommodate mixed-precision activation processing. This unified design maximizes PE utilization and enables fine-grained adaptation to the diverse arithmetic requirements of linear and attention workloads.

The proposed PE unit comprises two sub-PE wrappers, a shared accumulator, and dual register files for buffering activations. Each wrapper integrates two sub-PEs with integer-based compute units capable of executing mixed-precision dot-products on 32 pairs of 4-bit and 8-bit operands in parallel. The shared accumulator is time-multiplexed between wrappers

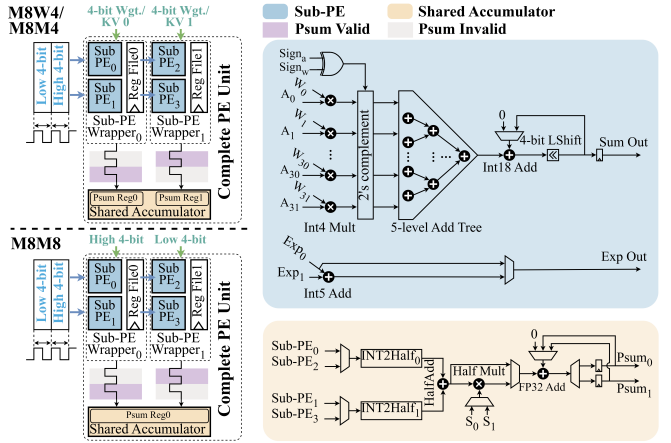


Fig. 13. Architecture of the reconfigurable PE unit supporting mixed-format and mixed-precision modes.

to aggregate cross-group results, amortizing the cost of FP operations while maintaining throughput.

When operating in M8W4 or M8M4 mode, each sub-PE independently performs MACs on 32-element pairs, forwarding partial sums to the shared accumulator for cross-group accumulation. The accumulator then converts integer outputs to FP16 according to their exponents. In M8W4 mode, the FP16 values are further scaled by the group-wise weight factor, while this step is bypassed in M8M4. The systolic propagation of activations allows the accumulator to be shared between two wrappers, improving hardware utilization. In M8M8 mode, both wrappers execute M8M4 computation in parallel, processing the high- and low-4-bit mantissas, respectively. Then, their results are fused in the accumulator to produce the final output.

C. Real-time BFP Converter

The BFP converter is a key component that transforms various activation types into BFP formats with different mantissa precisions, as described in Sec. III-B. Tightly integrated with the PE array’s output dataflow, it forms a deeply pipelined path that overlaps computation and conversion, effectively hiding latency. Because different activations use distinct configurations, the converter is carefully designed to handle varying conversion flows efficiently.

Fig. 14 illustrates two BFP conversion dataflows. All PEs in the same column produce valid results within the same cycle, while outputs from different columns propagate row-wise in a systolic fashion, aligning with the activations’ per-token dimension. For example, results from columns 0 to 15 become valid sequentially from T_0 to T_{15} . To exploit this pattern, as shown in Fig. 14(b), we design two dedicated conversion paths optimized for different activation types. V-type activations are processed spatially in parallel, while others follow a temporally serialized path.

Specifically, for V-type activations grouped per channel with a group size of 32, as shown in the upper left of Fig. 14(c), all eight results within a column (e.g., $C_{0,0}$ - $C_{7,0}$) are fed into a comparator tree simultaneously to identify the local maximum

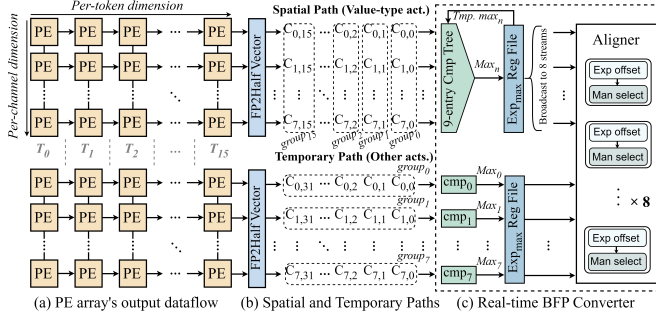


Fig. 14. Illustration of (a) output dataflow of the PE array, (b) two data paths supported by the BFP conversion framework, (c) architecture of the BFP converter.

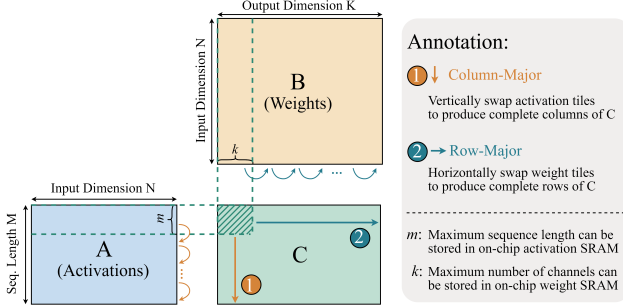


Fig. 15. Configurable output dataflows: column-major and row-major modes.

exponent. Since each group contains 32 elements, four output loops are required to obtain the final maximum exponent. The 32 elements of each group are then divided into four 8-element subgroups, which are forwarded to the aligner along with the derived maximum exponent. Each step processes 8 mantissas in parallel to produce the converted results.

In contrast, for per-token grouped activations, each PE row is equipped with a dedicated exponent comparator. As shown in the lower left of Fig. 14(c), results generated in a systolic fashion within a row are streamed directly into the comparator to identify the group's maximum exponent. After processing 32 results, the final maximum exponent for that row is obtained. Subsequently, the outputs from all eight rows are concurrently forwarded to the aligner, where each row performs mantissa alignment independently in a temporally serialized manner.

Notably, the aligner is shared across the two conversion paths for different activation types, enabling efficient hardware reuse. Furthermore, our proposed real-time BFP converter delivers similar compression effectiveness while achieving a 5.83 \times reduction in hardware area compared with the online quantizer introduced in the SOTA quantization-based LLM accelerator [24].

D. Tiling-aware Dataflow Design

Due to the limited capacity of on-chip SRAM, tiling strategies are widely adopted to efficiently support large-scale matrix multiplication. As illustrated in Fig. 15, consider multiplying a matrix A of size $M \times N$ with a matrix B of size $N \times K$, resulting in an output matrix C of size $M \times K$. When adopting dataflow 1 (column-major output flow) to compute matrix C, the total number of EMA for matrices

A and B is $\frac{K}{k} \times (M \times N) + N \times K$. In contrast, using dataflow 2 (row-major output flow) results in the total number is $\frac{M}{m} \times (N \times K) + (M \times N)$. Taking the linear layer as an example, for a given model, N and K are fixed, while k and m are determined by the on-chip resource allocation and thus remain constant. However, in practical LLM workloads, the number of input tokens can vary substantially, resulting in a wide dynamic range of M . Consequently, the choice between the two dataflows directly impacts the EMA cost under different workloads. Specifically, as M increases, the number of EMA of dataflow 2 gradually approaches and eventually becomes lower than that of dataflow 1.

Therefore, we design a flexible data generation flow (FDGF) controller that can switch between column-major and row-major dataflows through lightweight configuration. This controller manages the read address order of two data dispatchers from on-chip SRAM and coordinates on/off-chip data exchanges. Specifically, under the column-major dataflow, weights remain in on-chip SRAM until all activations are processed, after which the next weight column is fetched from off-chip memory. Conversely, in the row-major dataflow, activations stay on-chip until computation with all weights is completed before being replaced with new activations. This adaptability enables the architecture to select the most memory-efficient dataflow for a given workload, reducing costly EMA and further improving overall system efficiency.

V. EVALUATION

A. Experimental Setup

Software Implementation: We implement our proposed algorithm using PyTorch and Hugging Face libraries. The activation quantization (BFP) is implemented with the proposed Harmonia framework and the weight quantization (INT) is realized with the Omnipoint [54] framework. To demonstrate its effectiveness and generality, we benchmark three representative families of open-source LLMs: OPT [68], Llama [59], and Mistral [27], covering both pretrained models (e.g., OPT-6.7B) and instruction fine-tuned models (e.g., Llama-3.1-8B-Instruct). For pretrained models, we report zero-shot perplexity (PPL) on WikiText2 [48]. For instruction fine-tuned models, we evaluate on various tasks from LongBench [4], including summarization, few-shot

TABLE I
PERPLEXITY ON WIKITEXT2. LOWER IS BETTER. BFP(X) DENOTES AN X-BIT MANTISSA PRECISION.

Method	Linear		Atten.		Llama		Llama-2		OPT		KV
	Act.	Wgt.	Act.	KV	7B	13B	7B	13B	6.7B	Reduction	
Full	FP16	FP16	FP16	FP16	5.68	5.09	5.47	4.88	10.86	0.00%	
Omniquant	FP16	INT4	FP16	FP16	5.77	5.17	5.59	4.95	10.96	0.00%	
Tender	INT8	INT8	FP16	FP16	5.87	5.28	5.77	5.09	10.93	0.00%	
M-ANT	INT8	INT4	FP16	FP16	5.79	5.20	5.57	4.96	10.98	0.00%	
FIGNA	BFP16	INT4	FP16	FP16	5.78	5.18	5.60	4.96	10.96	0.00%	
Anda-m4	BFP4	INT4	FP16	FP16	7.45	6.36	8.26	6.43	12.30	0.00%	
Anda-m6	BFP6	INT4	FP16	FP16	5.86	5.26	5.70	5.06	11.01	0.00%	
Anda-m8	BFP8	INT4	FP16	FP16	5.79	5.19	5.60	4.97	10.96	0.00%	
Harmonia	BFP8	INT4	BFP8	BFP8	5.78	5.18	5.59	4.96	10.96	43.75%	
Harmonia	BFP8	INT4	BFP8	BFP4	6.19	5.51	5.90	5.20	11.69	68.75%	

TABLE II
ACCURACY RESULTS ON MULTIPLE BENCHMARKS FROM LONGBENCH v1 (WITH CONTEXT LENGTH SET TO 4K). HIGHER IS BETTER.

		2wikimqa	repobenchp	hotpotqa	trec	multinews	multifieldqa	qasper	qmsum	triviaqa	AVG.
Llama-3.2-1B-Instruct	Full	30.09	44.06	25.86	59.50	26.08	40.37	20.65	21.00	79.71	38.59
	Omniquant	26.95	42.63	25.11	57.00	25.43	38.98	20.67	20.50	72.01	36.59
	KIVI-q	23.35	37.42	26.17	53.50	10.28	35.78	11.93	18.24	68.45	31.68
	Harmonia-Naïve	11.50	32.07	9.78	43.00	18.36	26.95	10.15	14.47	44.19	23.39
	Harmonia	26.37	41.05	21.38	56.00	22.70	37.55	20.75	20.57	72.03	35.38
Llama-3.2-3B-Instruct	Full	34.85	48.97	38.45	68.00	26.52	46.99	35.06	20.97	87.71	45.28
	Omniquant	31.18	52.70	34.73	64.50	25.85	46.97	32.82	21.00	86.86	44.07
	KIVI-q	33.60	54.07	35.94	64.50	10.64	44.10	29.20	20.07	85.74	41.98
	Harmonia-Naïve	29.03	42.44	26.54	60.50	25.18	39.83	26.17	20.00	81.06	38.97
	Harmonia	32.76	53.58	36.67	63.00	24.85	44.87	30.49	21.61	89.14	44.11
Mistral-7B-Instruct-v0.3	Full	31.87	54.28	36.11	73.50	26.52	48.81	32.00	21.90	88.76	45.97
	Omniquant	26.88	53.14	33.77	74.50	27.04	46.98	30.52	22.13	89.28	44.92
	KIVI-q	27.28	52.29	35.69	73.50	8.33	43.78	30.01	16.26	89.03	41.80
	Harmonia-Naïve	30.82	48.42	38.42	70.50	27.07	42.17	28.45	21.35	87.04	43.80
	Harmonia	27.34	51.98	34.33	71.50	26.61	45.74	31.65	22.12	88.98	44.47
Llama-3.1-8B-Instruct	Full	35.23	56.29	39.04	70.00	27.21	49.67	40.24	20.96	89.01	47.52
	Omniquant	33.70	52.15	36.19	71.50	27.19	48.95	41.70	20.98	84.75	46.35
	KIVI-q	32.47	36.05	38.60	70.50	10.89	46.02	38.88	20.06	86.32	42.20
	Harmonia-Naïve	28.29	31.95	33.04	68.50	26.63	41.69	35.49	21.48	83.96	41.23
	Harmonia	34.34	55.15	41.45	66.50	25.74	47.61	38.73	20.91	90.26	46.74
Llama-2-13B-chat	Full	13.21	49.90	12.49	68.50	26.56	27.20	17.09	20.89	87.75	35.95
	Omniquant	14.70	45.95	16.31	67.00	25.81	26.94	14.57	20.09	87.31	35.41
	KIVI-q	9.91	47.14	8.03	65.00	8.30	12.51	11.34	10.68	85.60	28.72
	Harmonia-Naïve	13.06	36.26	10.30	55.50	23.77	25.38	14.38	17.65	68.48	29.42
	Harmonia	14.32	44.54	13.79	67.50	25.58	26.30	15.68	20.03	86.84	34.95

learning, document question answering, and code completion.

Algorithm Baselines: We compare our algorithm against strong baselines that employ either quantization schemes or BFP-based conversion approaches. For PPL evaluation on WikiText2, we consider: (a) Omnipoint [54], an algorithm that quantizes weights to 4 bits with a group size of 128 while keeping activations in FP16 format. (b) Tender [36], an accelerator that adopts offline activation quantization. (c) M-ANT [24], an accelerator utilizing online group-wise activation quantization. (d) FIGNA [25], a hardware framework which enhances numerical accuracy via BFP conversion with extended mantissa precision. (e) Anda [16], an accelerator supporting variable mantissa lengths under BFP-based scheme.

To further evaluate accuracy in more practical scenarios, we evaluate on LongBench. In this setting, we retain the baseline (a) and include KIVI [46], a SOTA algorithm targeting KV cache quantization to reduce memory footprint. We also conduct an ablation study by disabling the asymmetric bit allocation strategy and the offline-online hybrid outlier smoothing technique detailed in Sec. III. This comprehensive setup enables a rigorous assessment of our algorithm.

Hardware Implementation: Harmonia is implemented at the RTL level in SystemVerilog and functionally verified using VCS and Verdi. The prototype is synthesized with Design Compiler using TSMC 28nm process at a clock frequency of 300MHz and a supply voltage of 0.9V. Post-synthesis power analysis is performed in PrimeTime PX using value change dump (VCD) files generated based on the gate-level netlist simulations. On-chip SRAMs are generated using the TSMC-28nm memory compiler, while off-chip memory is modeled as HBM2 with an access energy of 3.9 pJ/bit and a bandwidth of 256 GB/s [30].

The synthesis results show that Harmonia occupies an area of 3.53mm² with a total power of 542 mW. It achieves a peak energy efficiency of 4534 GOPS/W in M8W4/M8M4 mode, and 2267 GOPS/W in M8M8 mode, demonstrating high

efficiency under different configurations.

Accelerator Baselines: To demonstrate the advantages of Harmonia, we compare it against several representative accelerator baselines, each employing distinct strategies for weight-only quantized LLM inference: (a) FP-FP engine, an FP16-based TPU-like [31] accelerator; (b) FP-INT engine, a systolic array with customized FP-INT compute units; (c) FIGNA and FIGNA-C [25], integer-based bit-parallel FP-INT accelerators preserving numerical accuracy; and (d) Anda [16], a bit-serial design supporting variable mantissa precision. All baselines are re-implemented and synthesized under the same technology node, frequency, and voltage as Harmonia for fair comparison. We further develop a cycle-accurate simulator building upon ANT [20] and DNNWeaver [55] to evaluate the energy and performance of all accelerators.

B. Model Accuracy Evaluation

For PPL evaluation, we report results under two KV cache precision settings: a conservative 8-bit and an aggressive 4-bit configuration, as shown in Table I. With 8-bit mantissas, our method achieves near-lossless accuracy while reducing KV-cache storage by 43.75%, whereas all baselines still use FP16 for attention computation and KV-cache storage. Further truncating the mantissas to 4 bits causes a moderate accuracy drop but yields a 68.75% reduction in storage, representing a practical trade-off between accuracy and memory efficiency.

We further evaluate five instruction-tuned models ranging from 1B to 13B parameters. To better reflect real-world scenarios, their performance is assessed on the LongBench benchmark suite, as summarized in Table II. The original KIVI method quantizes only the KV-cache while keeping weights and other activations in FP16 format, making a direct comparison unfair. To ensure consistency, we implement an extended variant, KIVI-q, which matches the bit-width settings of both weights and activations to those used in Harmonia.

As shown in Table II, our approach incurs only a 0.3% average accuracy drop across five evaluated models compared

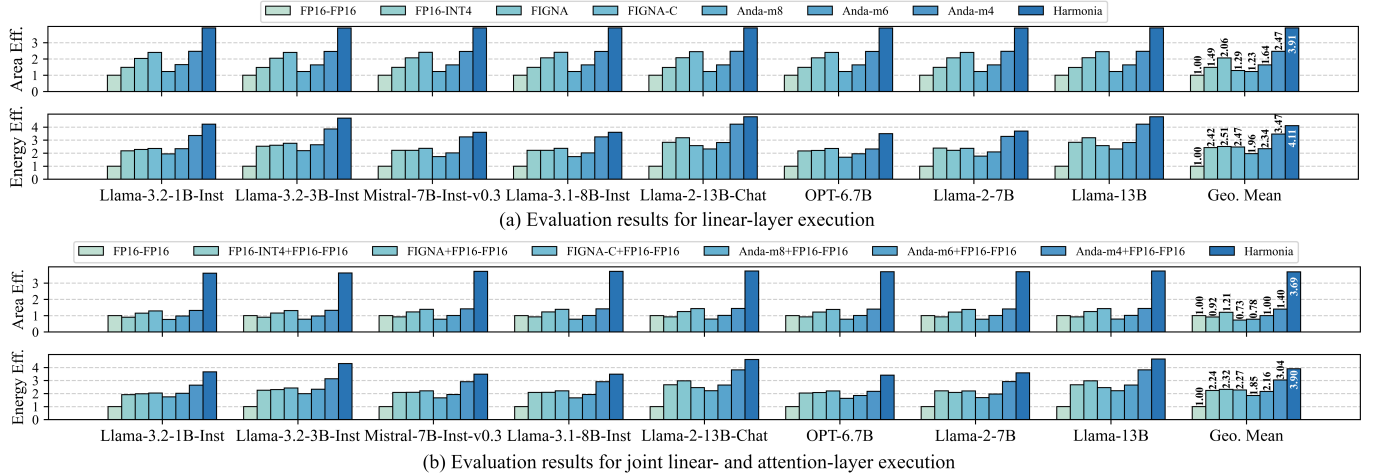


Fig. 16. Area efficiency and energy efficiency comparison across accelerators in (a) linear-layer execution and (b) joint linear- and attention-layer execution.

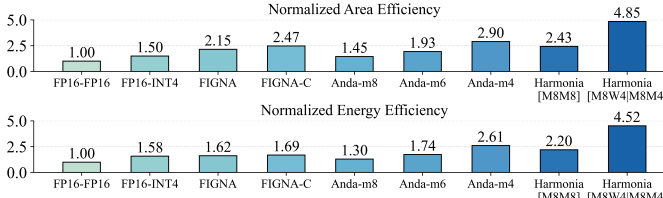


Fig. 17. PE-level comparison of area efficiency and energy efficiency, with all results normalized to the FP16-FP16 baseline.

with the weight-only quantization baseline, while delivering significant gains in both computation and memory efficiency. Notably, for Llama-3.2-3B-Instruct and Llama-3.1-8B-Instruct, it even surpasses the baseline accuracy, demonstrating its advantage. Moreover, compared with KIVI-q, Harmonia achieves a 3.9% average accuracy improvement. The ablation study further shows a 5.8% gain over the naïve version, confirming the effectiveness of our algorithm in mitigating accuracy degradation under aggressive compression.

C. PE-level Hardware Evaluation

We quantitatively compare the PE unit of Harmonia with hardware baselines in terms of area efficiency and energy efficiency. To ensure fairness, identical dot-product workloads extracted from real-world LLM inference are executed on each PE. The results, shown in Fig. 17, report area efficiency (TOPS/mm²) and energy efficiency (TOPS/W), respectively. Here, Anda-m(x) denotes the Anda PE configured with an x-bit mantissa precision.

Harmonia supports three operating modes: M8W4, M8M4, and M8M8, which differ in their internal parallelism and resource utilization. In the M8W4/M8M4 mode, two sub-PE wrappers in the PE independently perform 64 MACs in parallel, yielding a total throughput of 128 MACs per PE. In contrast, in the M8M8 mode, the two wrappers collaboratively execute 64 MACs over the same number of clock cycles. Consequently, the energy efficiency and area efficiency in the M8M8 mode are half of those in the M8W4/M8M4 mode.

As shown in Fig. 17, in M8W4/M8M4 mode, Harmonia achieves 1.67-4.85× higher area efficiency and 1.73-4.52× higher energy efficiency than baseline designs. In M8M8

mode, its area efficiency is slightly below FIGNA-C and Anda-m4, while energy efficiency remains comparable. These results demonstrate the scalability and flexibility of Harmonia across different precision configurations, effectively balancing among throughput, area and energy. This reconfigurable PE unit thus forms the foundation for system-level improvements in performance and efficiency.

D. System-level Hardware Evaluation

For a fair iso-area comparison, each baseline accelerator is configured with a PE array occupying the same silicon area as that of Harmonia, while maintaining identical on-chip SRAM capacity and operating frequency. During evaluation, we deploy various LLM workloads with a batch size of 1 and a sequence length of 2048 tokens. The analysis focuses on the prefill stage, measuring area efficiency, energy efficiency, speedup, and energy breakdown in two scenarios: (1) GEMM operations in linear layers only, and (2) GEMM executed jointly in both linear and attention layers. Since all accelerators except the FP16-FP16 engine and Harmonia lack native support for attention-layer computation, an auxiliary FP16-FP16 unit is integrated to handle attention layers for functional completeness. The linear-layer evaluation results are presented in Fig. 16(a) and Fig. 18(a), while Fig. 16(b) and Fig. 18(b) show results for joint linear-attention execution.

Results from the linear-layer evaluation show that Harmonia achieves a 1.58-3.91× higher area efficiency and 1.18-4.11× improvement in energy efficiency on average, while delivering up to 4.89× speedup and reducing total energy consumption by 4.15× compared with the FP16-FP16 baseline. When GEMM operations in both linear and attention layers are considered, Harmonia achieves up to 5.05× and 3.90× improvements in area efficiency and energy efficiency, respectively. Meanwhile, it delivers an average 2.17-4.62× speedup and reduces average energy consumption by 1.27-3.99× compared with baselines.

To further validate the versatility of Harmonia, we evaluate its performance across varying sequence lengths. Fig. 19 presents the normalized execution cycles and energy of Harmonia and baseline accelerators using the Llama-3.2-3B-

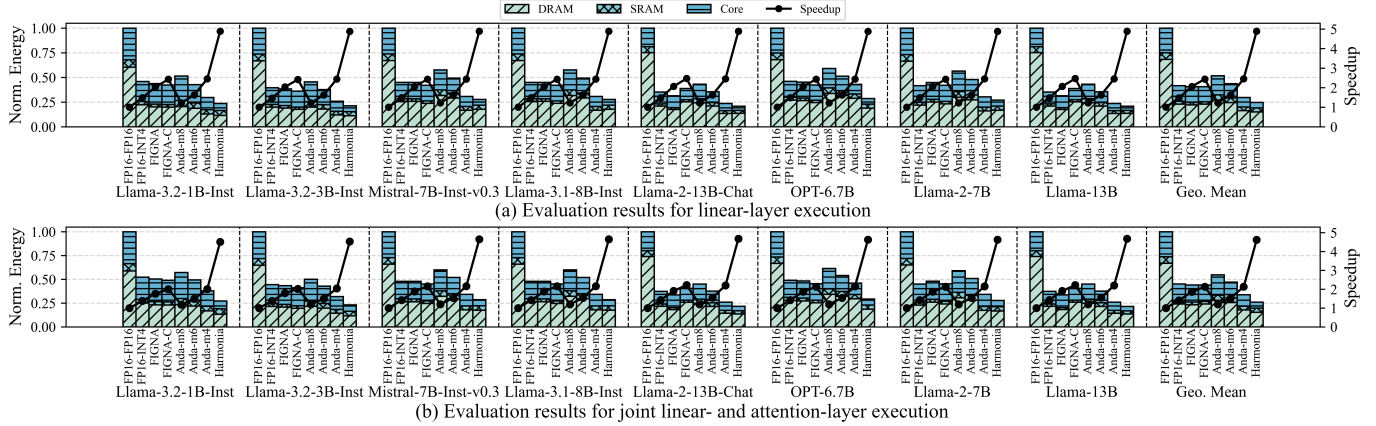


Fig. 18. Speedup and energy breakdown comparison across accelerators in (a) linear-layer execution and (b) joint linear- and attention-layer execution.

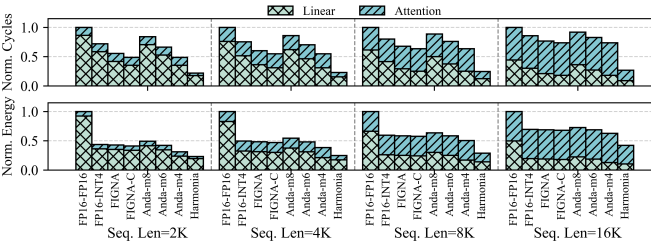


Fig. 19. Speedup and energy comparison across accelerators under varying sequence lengths.

Instruct model with sequence lengths from 2K to 16K. As the sequence length grows, the attention layer gradually becomes dominant. With unified optimization for both linear and attention operations, Harmonia consistently outperforms all baselines, achieving significant reductions in execution cycles and energy consumption. Specifically, from 2K to 16K tokens, Harmonia delivers 2.50-4.14x speedup and 1.54-3.35x energy reduction, demonstrating strong scalability and efficiency across varying workloads.

The performance gains mainly stem from two key factors: (1) **Reconfigurable compute core design**: Harmonia features a reconfigurable PE array that unifies mixed-type and mixed-precision computation in linear and attention layers. It flexibly composes mixed-precision operations from 4-bit basic building blocks and time-multiplexes shared accumulators between wrappers, achieving high utilization with minimal area cost. Compared with FIGNA’s wide-bit parallel MAC units and Anda’s bit-serial design, Harmonia strikes a balance among area, power, and throughput. (2) **Compressed activation representation**: Harmonia adopts a mixed-precision, mantissa-compressed BFP format for activation conversion and storage. Using an asymmetric bit-allocation strategy that truncates mantissas to 8 or 4 bits, it greatly reduces memory access overhead and further improves overall energy efficiency.

VI. RELATED WORK AND DISCUSSION

LLM accelerators. To mitigate the high computational and memory costs of LLMs, many accelerators have been proposed, mainly focusing on weight-only or weight-activation quantization. For weight-only quantization, [25], [16] convert FP activations to the BFP format to enable integer-based

FP-INT computation, while [52], [49] employ LUT-based arithmetic. However, these designs primarily optimize linear layers and ignore the costly FP-FP computations in attention modules. Later efforts [7], [19], [36], [24] quantize activations to further reduce overhead, but activation quantization is challenging: offline quantization often degrades accuracy, while dynamic quantization requires expensive runtime scaling and offset computation. In contrast, Harmonia extends the BFP format to activations in both linear and attention layers, which together dominate over 90% of LLM computation, reducing the cost of activation compression compared with dynamic quantization and striking a balance between model accuracy and hardware efficiency.

KV cache optimization. During auto-regressive generation, frequent access to the KV cache causes heavy memory and bandwidth pressure, especially in long-context scenarios. Existing methods, such as KV cache quantization [66], [57], [23], [39], reduce storage but introduce runtime overhead. Harmonia instead represents the KV cache in the BFP format, achieving similar compression with lower hardware cost. Moreover, this approach is orthogonal to other techniques, such as eviction [71], [45], [73], and sliding window [15], [64], allowing further compression when combined.

VII. CONCLUSION

This work presents Harmonia, an algorithm-hardware co-design framework that converts activations in both linear and attention layers into the BFP format, and integrates efficient reconfigurable hardware units to support mixed-precision BFP-INT and BFP-BFP operations for weight-only quantized LLMs. We achieve this by carefully selecting a BFP configuration with a group size of 32 and a mantissa length of 8 to preserve model accuracy. Building on this foundation, we introduce an asymmetric bit-allocation and offline-online hybrid outlier smoothing technique, compressing the KV cache to 31.25% of its original size, reducing both memory footprint and access overhead. To fully leverage algorithmic benefits, we design complementary hardware components, including a reconfigurable mixed-precision PE array, a real-time BFP converter, and a flexible tiling-aware dataflow. Comprehensive evaluations demonstrate that Harmonia achieves a 3.08x

speedup, a $3.84\times$ improvement in area efficiency, and a $2.03\times$ enhancement in energy efficiency on average over prior works. These results highlight Harmonia’s adaptability for efficiently handling diverse LLM workloads.

REFERENCES

[1] M. Abdin, J. Aneja, H. Behl, S. Bubeck, R. Eldan, S. Gunasekar, M. Harrison, R. J. Hewett, M. Javaheripi, P. Kauffmann, J. R. Lee, Y. Tat Lee, Y. Li, W. Liu, C. C. T. Mendes, A. Nguyen, E. Price, G. de Rosa, O. Saarikivi, A. Salim, S. Shah, X. Wang, R. Ward, Y. Wu, D. Yu, C. Zhang, and Y. Zhang, “Phi-4 technical report,” *arXiv preprint arXiv:2412.08905*, 2024.

[2] M. Adnan, A. Arunkumar, G. Jain, P. J. Nair, I. Soloveychik, and P. Kamath, “Keyformer: Kv cache reduction through key tokens selection for efficient generative inference,” *Proceedings of Machine Learning and Systems*, vol. 6, pp. 114–127, 2024.

[3] S. Ashkboos, A. Mohtashami, M. L. Croci, B. Li, P. Cameron, M. Jaggi, D. Alistarh, T. Hoefler, and J. Hensman, “Quarot: Outlier-free 4-bit inference in rotated llms,” *Advances in Neural Information Processing Systems*, vol. 37, pp. 100213–100240, 2024.

[4] Y. Bai, X. Lv, J. Zhang, H. Lyu, J. Tang, Z. Huang, Z. Du, X. Liu, A. Zeng, L. Hou, Y. Dong, J. Tang, and J. Li, “Longbench: A bilingual, multitask benchmark for long context understanding,” in *Proceedings of the 62nd Annual Meeting of the Association for Computational Linguistics (Volume 1: Long Papers)*, 2024, pp. 3119–3137.

[5] Y. Bai, S. Tu, J. Zhang, H. Peng, X. Wang, X. Lv, S. Cao, J. Xu, L. Hou, Y. Dong, J. Tang, L. Hou, and J. Li, “Longbench v2: Towards deeper understanding and reasoning on realistic long-context multitasks,” in *Proceedings of the 63rd Annual Meeting of the Association for Computational Linguistics (Volume 1: Long Papers)*, 2025, pp. 3639–3664.

[6] T. Brown, B. Mann, N. Ryder, M. Subbiah, J. D. Kaplan, P. Dhariwal, A. Neelakantan, P. Shyam, G. Sastry, A. Askell, S. Agarwal, A. Herbert-Voss, G. Krueger, T. Henighan, R. Child, A. Ramesh, D. M. Ziegler, J. Wu, C. Winter, C. Hesse, M. Chen, E. Sigler, M. Litwin, S. Gray, B. Chess, J. Clark, C. Berner, S. McCandlish, A. Radford, I. Sutskever, and D. Amodei, “Language models are few-shot learners,” *Advances in neural information processing systems*, vol. 33, pp. 1877–1901, 2020.

[7] Y. Chen, A. F. AbouElhamayed, X. Dai, Y. Wang, M. Andronic, G. A. Constantinides, and M. S. Abdelfattah, “Bitmod: Bit-serial mixture-of-datatype llm acceleration,” in *2025 IEEE International Symposium on High Performance Computer Architecture (HPCA)*. IEEE, 2025, pp. 1082–1097.

[8] A. Chowdhery, S. Narang, J. Devlin, M. Bosma, G. Mishra, A. Roberts, P. Barham, H. W. Chung, C. Sutton, S. Gehrmann, P. Schuh, K. Shi, S. Tsvyashchenko, J. Maynez, A. Rao, P. Barnes, Y. Tay, N. Shazeer, V. Prabhakaran, E. Reif, N. Du, B. Hutchinson, R. Pope, J. Bradbury, J. Austin, M. Isard, G. Gur-Ari, P. Yin, T. Duke, A. Levskaya, S. Ghemawat, S. Dev, H. Michalewski, X. Garcia, V. Misra, K. Robinson, L. Fedus, D. Zhou, D. Ippolito, D. Luan, H. Lim, B. Zoph, A. Spiridonov, R. Sepassi, D. Dohan, S. Agrawal, M. Omernick, A. M.Dai, T. Sankaranarayana Pillai, M. Pellat, A. Lewkowycz, E. Moreira, R. Child, O. Polozov, K. Lee, Z. Zhou, X. Wang, B. Saeta, M. Diaz, O. Firat, M. Catasta, J. Wei, K. Meier-Hellstern, D. Eck, J. Dean, S. Petrov, and N. Fiedel, “Palm: Scaling language modeling with pathways,” *Journal of Machine Learning Research*, vol. 24, no. 240, pp. 1–113, 2023.

[9] B. Darvish Rouhani, R. Zhao, V. Elango, R. Shafipour, M. Hall, M. Mesmakhosroshahi, A. More, L. Melnick, M. Golub, G. Varatkar, L. Shao, G. Kolhe, D. Melts, J. Klar, R. L’Heureux, M. Perry, D. Burger, E. Chung, Z. Deng, S. Naghshineh, J. Park, and M. Naumov, “With shared microexponents, a little shifting goes a long way,” in *Proceedings of the 50th Annual International Symposium on Computer Architecture*, 2023, pp. 1–13.

[10] DeepSeek-AI, A. Liu, B. Feng, B. Xue, B. Wang, B. Wu, C. Lu, C. Zhao, C. Deng, C. Zhang, C. Ruan, D. Dai, D. Guo, D. Yang, D. Chen, D. Ji, E. Li, F. Lin, F. Dai, F. Luo, G. Hao, G. Chen, G. Li, H. Zhang, H. Bao, H. Xu, H. Wang, H. Zhang, H. Ding, H. Xin, H. Gao, H. Li, H. Qu, J. L. Cai, J. Liang, J. Guo, J. Ni, J. Li, J. Wang, J. Chen, J. Chen, J. Yuan, J. Qiu, J. Li, J. Song, K. Dong, K. Hu, K. Gao, K. Guan, K. Huang, K. Yu, L. Wang, L. Zhang, L. Xu, L. Xia, L. Zhao, L. Wang, L. Zhang, M. Li, M. Wang, M. Zhang, M. Zhang, M. Tang, M. Li, N. Tian, P. Huang, P. Wang, P. Zhang, Q. Wang, Q. Zhu, Q. Chen, Q. Du, R. J. Chen, R. L. Jin, R. Ge, R. Zhang, R. Pan, R. Wang, R. Xu, R. Zhang, R. Chen, S. S. Li, S. Lu, S. Zhou, S. Chen, S. Wu, S. Ye, S. Ye, S. Ma, S. Wang, S. Zhou, S. Yu, S. Zhou, S. Pan, T. Wang, T. Yun, T. Pei, T. Sun, W. L. Xiao, W. Zeng, W. Zhao, W. An, W. Liu, W. Liang, W. Gao, W. Yu, W. Zhang, X. Q. Li, X. Jin, X. Wang, X. Bi, X. Liu, X. Wang, X. Shen, X. Chen, X. Zhang, X. Chen, X. Nie, X. Sun, X. Wang, X. Cheng, X. Liu, X. Xie, X. Liu, X. Yu, X. Song, X. Shan, X. Zhou, X. Yang, X. Li, X. Su, X. Lin, Y. K. Li, Y. Q. Wang, Y. X. Wei, Y. X. Zhu, Y. Zhang, Y. Xu, Y. Xu, Y. Huang, Y. Li, Y. Zhao, Y. Sun, Y. Li, Y. Wang, Y. Yu, Y. Zheng, Y. Zhang, Y. Shi, Y. Xiong, Y. He, Y. Tang, Y. Piao, Y. Wang, Y. Tan, Y. Ma, Y. Liu, Y. Guo, Y. Wu, Y. Ou, Y. Zhu, Y. Wang, Y. Gong, Y. Zou, Y. He, Y. Zha, Y. Xiong, Y. Ma, Y. Yan, Y. Luo, Y. You, Y. Liu, Y. Zhou, Z. F. Wu, Z. Z. Ren, Z. Ren, Z. Sha, Z. Fu, Z. Xu, Z. Huang, Z. Zhang, Z. Xie, Z. Zhang, Z. Hao, Z. Gou, Z. Ma, Z. Yan, Z. Shao, Z. Xu, Z. Wu, Z. Zhang, Z. Li, Z. Gu, Z. Zhu, Z. Liu, Z. Li, Z. Xie, Z. Song, Z. Gao, and Z. Pan, “Deepseek-v3 technical report,” *arXiv preprint arXiv:2412.19437*, 2024.

[11] T. Dettmers, M. Lewis, Y. Belkada, and L. Zettlemoyer, “Gpt3. int8 (): 8-bit matrix multiplication for transformers at scale,” *Advances in neural information processing systems*, vol. 35, pp. 30318–30332, 2022.

[12] T. Dettmers, R. Svirshevski, V. Egiazarian, D. Kuznedelev, E. Frantar, S. Ashkboos, A. Borzunov, T. Hoefler, and D. Alistarh, “Spqr: A sparse-quantized representation for near-lossless llm weight compression,” *arXiv preprint arXiv:2306.03078*, 2023.

[13] T. Dettmers and L. Zettlemoyer, “The case for 4-bit precision: k-bit inference scaling laws,” in *International Conference on Machine Learning*. PMLR, 2023, pp. 7750–7774.

[14] Y. Ding, L. L. Zhang, C. Zhang, Y. Xu, N. Shang, J. Xu, F. Yang, and M. Yang, “Longrope: Extending llm context window beyond 2 million tokens,” *arXiv preprint arXiv:2402.13753*, 2024.

[15] H. Duanmu, Z. Yuan, X. Li, J. Duan, X. Zhang, and D. Lin, “Skvq: Sliding-window key and value cache quantization for large language models,” *arXiv preprint arXiv:2405.06219*, 2024.

[16] C. Fang, M. Shi, R. Geens, A. Symons, Z. Wang, and M. Verhelst, “Anda: Unlocking efficient llm inference with a variable-length grouped activation data format,” in *2025 IEEE International Symposium on High Performance Computer Architecture (HPCA)*. IEEE, 2025, pp. 1467–1481.

[17] E. Frantar, S. Ashkboos, T. Hoefler, and D. Alistarh, “Gptq: Accurate post-training quantization for generative pre-trained transformers,” *arXiv preprint arXiv:2210.17323*, 2022.

[18] C. Guo, B. Lou, X. Liu, D. Boland, P. H. Leong, and C. Zhuo, “Boost: Block minifloat-based on-device cnn training accelerator with transfer learning,” in *2023 IEEE/ACM International Conference on Computer Aided Design (ICCAD)*. IEEE, 2023, pp. 1–9.

[19] C. Guo, J. Tang, W. Hu, J. Leng, C. Zhang, F. Yang, Y. Liu, M. Guo, and Y. Zhu, “Olive: Accelerating large language models via hardware-friendly outlier-victim pair quantization,” in *Proceedings of the 50th Annual International Symposium on Computer Architecture*, 2023, pp. 1–15.

[20] C. Guo, C. Zhang, J. Leng, Z. Liu, F. Yang, Y. Liu, M. Guo, and Y. Zhu, “Ant: Exploiting adaptive numerical data type for low-bit deep neural network quantization,” in *2022 55th IEEE/ACM International Symposium on Microarchitecture (MICRO)*. IEEE, 2022, pp. 1414–1433.

[21] J. Hoffmann, S. Borgeaud, A. Mensch, E. Buchatskaya, T. Cai, E. Rutherford, D. d. L. Casas, L. A. Hendricks, J. Welbl, A. Clark, T. Hennigan, E. Noland, K. Millican, G. v. d. Driessche, B. Damoc, A. Guy, S. Osindero, K. Simonyan, E. Elsen, J. W.Rae, O. Vinyals, and L. Sifre, “Training compute-optimal large language models,” *arXiv preprint arXiv:2203.15556*, 2022.

[22] K. Hong, G. Dai, J. Xu, Q. Mao, X. Li, J. Liu, K. Chen, Y. Dong, and Y. Wang, “Flashdecoding++: Faster large language model inference with synchronization, flat gemm optimization, and heuristics,” *Proceedings of Machine Learning and Systems*, vol. 6, pp. 148–161, 2024.

[23] C. Hooper, S. Kim, H. Mohammadzadeh, M. W. Mahoney, Y. S. Shao, K. Keutzer, and A. Gholami, “Kvquant: Towards 10 million context length llm inference with kv cache quantization,” *Advances in Neural Information Processing Systems*, vol. 37, pp. 1270–1303, 2024.

[24] W. Hu, H. Zhang, C. Guo, Y. Feng, R. Guan, Z. Hua, Z. Liu, Y. Guan, M. Guo, and J. Leng, “M-ant: Efficient low-bit group quantization for llms via mathematically adaptive numerical type,” in *2025 IEEE International Symposium on High Performance Computer Architecture (HPCA)*. IEEE, 2025, pp. 1112–1126.

[25] J. Jang, Y. Kim, J. Lee, and J.-J. Kim, “Figna: Integer unit-based accelerator design for fp-int gemm preserving numerical accuracy,” in *2024 IEEE International Symposium on High-Performance Computer Architecture (HPCA)*. IEEE, 2024, pp. 760–773.

[26] A. Q. Jiang, A. Sablayrolles, A. Mensch, C. Bamford, D. S. Chaplot, D. de las Casas, F. Bressand, G. Lengyel, G. Lampe, L. Saulnier, L. R. Lavaud, M.-A. Lachaux, P. Stock, T. L. Scao, T. Lavril, T. Wang, T. Lacroix, and W. E. Sayed, "Mistral 7b," *arXiv preprint arXiv:2310.06825*, 2023.

[27] D. Jiang, Y. Liu, S. Liu, J. Zhao, H. Zhang, Z. Gao, X. Zhang, J. Li, and H. Xiong, "From clip to dino: Visual encoders shout in multi-modal large language models," *arXiv preprint arXiv:2310.08825*, 2023.

[28] Z. Jiang, H. Lin, Y. Zhong, Q. Huang, Y. Chen, Z. Zhang, Y. Peng, X. Li, C. Xie, S. Nong, Y. Jia, S. He, H. Chen, Z. Bai, Q. Hou, S. Yan, D. Zhou, Y. Sheng, Z. Jiang, H. Xu, H. Wei, Z. Zhang, P. Nie, L. Zou, S. Zhao, L. Xiang, Z. Liu, Z. Li, X. Jia, J. Ye, X. Jin, and X. Liu, "[MegaScale]: Scaling large language model training to more than 10,000 {GPUs}, " in *21st USENIX Symposium on Networked Systems Design and Implementation (NSDI 24)*, 2024, pp. 745–760.

[29] Z. Jiang, X. Ma, and W. Chen, "Longrag: Enhancing retrieval-augmented generation with long-context llms," *arXiv preprint arXiv:2406.15319*, 2024.

[30] N. P. Jouppi, D. H. Yoon, M. Ashcraft, M. Gottscho, T. B. Jablin, G. Kurian, J. Laudon, S. Li, P. Ma, X. Ma, T. Norrie, N. Patil, S. Prasad, C. Young, Z. Zhou, and D. Patterson, "Ten lessons from three generations shaped google's tpuv4i: Industrial product," in *2021 ACM/IEEE 48th Annual International Symposium on Computer Architecture (ISCA)*. IEEE, 2021, pp. 1–14.

[31] N. P. Jouppi, C. Young, N. Patil, D. Patterson, G. Agrawal, R. Bajwa, S. Bates, S. Bhatia, N. Boden, A. Borchers, R. Boyle, P.-l. Cantin, C. Chao, C. Clark, J. Coriell, M. Daley, M. Dau, J. Dean, B. Gelb, V. T. Ghaemmaghami, R. Gottipati, W. Gulland, R. Hagmann, C. R. Ho, D. Hogberg, J. Hu, R. Hundt, D. Hurt, J. Ibarz, A. Jaffey, A. Jaworski, A. Kaplan, H. Khaitan, D. Killebrew, A. Koch, N. Kumar, S. Lacy, J. Laudon, J. Law, D. Le, C. Leary, Z. Liu, K. Lucke, A. Lundin, G. AacKean, A. Maggiore, M. Mahony, K. Miller, R. Nagarajan, R. Narayanaswami, R. Ni, N. Nix, T. Norrie, M. Omernick, N. Penukonda, A. Phelps, J. Ross, M. Ross, A. Salek, E. Samadiani, C. Severn, G. Sizikov, M. Snelham, J. Souter, D. Steinberg, A. Swing, M. Tan, G. Thorson, B. Tian, H. Toma, E. Tuttle, V. Vasudevan, R. Walter, W. Wang, E. Wilcox, and D. H. Yoon, "In-datacenter performance analysis of a tensor processing unit," in *Proceedings of the 44th annual international symposium on computer architecture*, 2017, pp. 1–12.

[32] J. Kaplan, S. McCandlish, T. Henighan, T. B. Brown, B. Chess, R. Child, S. Gray, A. Radford, J. Wu, and D. Amodei, "Scaling laws for neural language models," *arXiv preprint arXiv:2001.08361*, 2020.

[33] M. Kim, S. Hong, R. Ko, S. Choi, H. Lee, J. Kim, J.-Y. Kim, and J. Park, "Oaken: Fast and efficient llm serving with online-offline hybrid kv cache quantization," in *Proceedings of the 52nd Annual International Symposium on Computer Architecture*, 2025, pp. 482–497.

[34] K. Kwon, Z. Li, S. Zhuang, Y. Sheng, L. Zheng, C. H. Yu, J. Gonzalez, H. Zhang, and I. Stoica, "Efficient memory management for large language model serving with paggedattention," in *Proceedings of the 29th symposium on operating systems principles*, 2023, pp. 611–626.

[35] C. Lee, J. Jin, T. Kim, H. Kim, and E. Park, "Owq: Outlier-aware weight quantization for efficient fine-tuning and inference of large language models," in *Proceedings of the AAAI Conference on Artificial Intelligence*, vol. 38, no. 12, 2024, pp. 13355–13364.

[36] J. Lee, W. Lee, and J. Sim, "Tender: Accelerating large language models via tensor decomposition and runtime requantization," in *2024 ACM/IEEE 51st Annual International Symposium on Computer Architecture (ISCA)*. IEEE, 2024, pp. 1048–1062.

[37] W. Lee, J. Lee, J. Seo, and J. Sim, "{InfiniGen}: Efficient generative inference of large language models with dynamic {KV} cache management," in *18th USENIX Symposium on Operating Systems Design and Implementation (OSDI 24)*, 2024, pp. 155–172.

[38] D. Li, B. Jiang, L. Huang, A. Beigi, C. Zhao, Z. Tan, A. Bhattacharjee, Y. Jiang, C. Chen, T. Wu, K. Shu, L. Cheng, and H. Liu, "From generation to judgment: Opportunities and challenges of llm-as-a-judge," in *Proceedings of the 2025 Conference on Empirical Methods in Natural Language Processing*, 2025, pp. 2757–2791.

[39] J. Li, Y. Zhang, M. Y. Hassan, T. Chafekar, T. Cai, Z. Ren, P. Guo, F. Karimzadeh, C. Wang, and C. Gan, "Commvg: Commutative vector quantization for kv cache compression," *arXiv preprint arXiv:2506.18879*, 2025.

[40] L. Li, Q. Li, B. Zhang, and X. Chu, "Norm tweaking: High-performance low-bit quantization of large language models," in *Proceedings of the AAAI Conference on Artificial Intelligence*, vol. 38, no. 17, 2024, pp. 18536–18544.

[41] H. Lin, H. Xu, Y. Wu, J. Cui, Y. Zhang, L. Mou, L. Song, Z. Sun, and Y. Wei, "Duquant: Distributing outliers via dual transformation makes stronger quantized llms," *Advances in Neural Information Processing Systems*, vol. 37, pp. 87766–87800, 2024.

[42] J. Lin, J. Tang, H. Tang, S. Yang, W.-M. Chen, W.-C. Wang, G. Xiao, X. Dang, C. Gan, and S. Han, "Awq: Activation-aware weight quantization for on-device llm compression and acceleration," *Proceedings of machine learning and systems*, vol. 6, pp. 87–100, 2024.

[43] Y. Lin, H. Tang, S. Yang, Z. Zhang, G. Xiao, C. Gan, and S. Han, "Qserve: W4a8kv4 quantization and system co-design for efficient llm serving," *arXiv preprint arXiv:2405.04532*, 2024.

[44] Z. Liu, C. Zhao, I. Fedorov, B. Soran, D. Choudhary, R. Krishnamoorthi, V. Chandra, Y. Tian, and T. Blankevoort, "Spinquant: Llm quantization with learned rotations," *arXiv preprint arXiv:2405.16406*, 2024.

[45] Z. Liu, A. Desai, F. Liao, W. Wang, V. Xie, Z. Xu, A. Kyrillidis, and A. Shrivastava, "Scissorhands: Exploiting the persistence of importance hypothesis for llm kv cache compression at test time," *Advances in Neural Information Processing Systems*, vol. 36, pp. 52342–52364, 2023.

[46] Z. Liu, J. Yuan, H. Jin, S. Zhong, Z. Xu, V. Braverman, B. Chen, and X. Hu, "Kivi: A tuning-free asymmetric 2bit quantization for kv cache," *arXiv preprint arXiv:2402.02750*, 2024.

[47] S. Ma, H. Wang, L. Ma, L. Wang, W. Wang, S. Huang, L. Dong, R. Wang, J. Xue, and F. Wei, "The era of 1-bit llms: All large language models are in 1.58 bits," *arXiv preprint arXiv:2402.17764*, vol. 1, no. 4, 2024.

[48] S. Merity, C. Xiong, J. Bradbury, and R. Socher, "Pointer sentinel mixture models," *arXiv preprint arXiv:1609.07843*, 2016.

[49] Z. Mo, L. Wang, J. Wei, Z. Zeng, S. Cao, L. Ma, N. Jing, T. Cao, J. Xue, F. Yang, and M. Yang, "Lut tensor core: A software-hardware co-design for lut-based low-bit llm inference," in *Proceedings of the 52nd Annual International Symposium on Computer Architecture*, 2025, pp. 514–528.

[50] S.-H. Noh, J. Koo, S. Lee, J. Park, and J. Kung, "Flexblock: A flexible dnn training accelerator with multi-mode block floating point support," *IEEE Transactions on Computers*, vol. 72, no. 9, pp. 2522–2535, 2023.

[51] OpenAI, J. Achiam, S. Adler, S. Agarwal, L. Ahmad, I. Akkaya, F. L. Aleman, D. Almeida, J. Altenschmidt, S. Altman, S. Anadkat, R. Avila, I. Babuschkin, S. Balaji, V. Balcom, P. Baltescu, H. Bao, M. Bavarian, J. Belgum, I. Bello, J. Berdine, G. Bernadett-Shapiro, C. Berner, L. Bogdonoff, O. Boiko, M. Boyd, A.-L. Brakman, G. Brockman, T. Brooks, M. Brundage, K. Button, T. Cai, R. Campbell, A. Cann, B. Carey, C. Carlson, R. Carmichael, B. Chan, C. Chang, F. Chantzis, D. Chen, S. Chen, R. Chen, J. Chen, M. Chen, B. Chess, C. Cho, C. Chu, H. W. Chung, D. Cummings, J. Currier, Y. Dai, C. Decareaux, T. Degry, N. Deutsch, D. Deville, A. Dhar, D. Dohan, S. Dowling, S. Dunning, A. Ecoffet, A. Eleti, T. Eloundou, D. Farhi, L. Fedus, N. Felix, S. P. Fishman, J. Forte, I. Fulford, L. Gao, E. Georges, C. Gibson, V. Goel, T. Gogineni, G. Goh, R. Gontijo-Lopes, J. Gordon, M. Grafstein, S. Gray, R. Greene, J. Gross, S. S. Gu, Y. Guo, C. Hallacy, J. Han, J. Harris, Y. He, M. Heaton, J. Heidecke, C. Hesse, A. Hickey, W. Hickey, P. Hoeschele, B. Houghton, K. Hsu, S. Hu, X. Hu, J. Huizinga, S. Jain, S. Jain, J. Jang, A. Jiang, R. Jiang, H. Jin, D. Jin, S. Jomoto, B. Jonn, H. Jun, T. Kaftan, Łukasz Kaiser, A. Kamali, I. Kanitscheider, N. S. Keskar, T. Khan, L. Kilpatrick, J. W. Kim, C. Kim, Y. Kim, J. H. Kirchner, J. Kirov, M. Knight, D. Kokotajlo, Łukasz Kondraciuk, A. Kondrich, A. Konstantinidis, K. Kosic, G. Krueger, V. Kuo, M. Lampe, I. Lan, T. Lee, J. Leike, J. Leung, D. Levy, C. M. Li, R. Lim, M. Lin, S. Lin, M. Litwin, T. Lopez, R. Lowe, P. Lue, A. Makanju, K. Malfacini, S. Manning, T. Markov, Y. Markovski, B. Martin, K. Mayer, A. Mayne, B. McGrew, S. M. McKinney, C. McLeavey, P. McMillan, J. McNeil, D. Medina, A. Mehta, J. Menick, L. Metz, A. Mishchenko, P. Mishkin, V. Monaco, E. Morikawa, D. Mossing, T. Mu, M. Murati, O. Murk, D. Mély, A. Nair, R. Nakano, R. Nayak, A. Neelakantan, R. Ngo, H. Noh, L. Ouyang, C. O'Keefe, J. Pachocki, A. Paino, J. Palermo, A. Pantuliano, G. Parascandolo, J. Parish, E. Parparita, A. Passos, M. Pavlov, A. Peng, A. Perelman, F. de Avila Belbute Peres, M. Petrov, H. P. de Oliveira Pinto, Michael Pokorny, M. Pokrass, V. H. Pong, T. Powell, A. Power, B. Power, E. Proehl, R. Puri, A. Radford, J. Rae, A. Ramesh, C. Raymond, F. Real, K. Rimbach, C. Ross, B. Rotsted, H. Roussez, N. Ryder, M. Saltarelli, T. Sanders, S. Santurkar, G. Sastry, H. Schmidt, D. Schnurr, J. Schulman, D. Selsam, K. Sheppard, T. Sherbakov,

J. Shieh, S. Shoker, P. Shyam, S. Sidor, E. Sigler, M. Simens, J. Sitkin, K. Slama, I. Sohl, B. Sokolowsky, Y. Song, N. Staudacher, F. P. Such, N. Summers, I. Sutskever, J. Tang, N. Tezak, M. B. Thompson, P. Tillet, A. Tootoonchian, E. Tseng, P. Tuggle, N. Turley, J. Tworek, J. F. C. Uribe, A. Vallone, A. Vijayvergiya, C. Voss, C. Wainwright, J. J. Wang, A. Wang, B. Wang, J. Ward, J. Wei, C. Weinmann, A. Welihinda, P. Welinder, J. Weng, L. Weng, M. Wiethoff, D. Willner, C. Winter, S. Wolrich, H. Wong, L. Workman, S. Wu, J. Wu, M. Wu, K. Xiao, T. Xu, S. Yoo, K. Yu, Q. Yuan, W. Zaremba, R. Zellers, C. Zhang, M. Zhang, S. Zhao, T. Zheng, J. Zhuang, W. Zhuk, and B. Zoph, “Gpt-4 technical report,” 2023.

[52] G. Park, H. Kwon, J. Kim, J. Bae, B. Park, D. Lee, and Y. Lee, “Figlut: An energy-efficient accelerator design for fp-int gemm using look-up tables,” in *2025 IEEE International Symposium on High Performance Computer Architecture (HPCA)*. IEEE, 2025, pp. 1098–1111.

[53] G. Park, B. Park, M. Kim, S. Lee, J. Kim, B. Kwon, S. J. Kwon, B. Kim, Y. Lee, and D. Lee, “Lut-gemm: Quantized matrix multiplication based on luts for efficient inference in large-scale generative language models,” *arXiv preprint arXiv:2206.09557*, 2022.

[54] W. Shao, M. Chen, Z. Zhang, P. Xu, L. Zhao, Z. Li, K. Zhang, P. Gao, Y. Qiao, and P. Luo, “Omniquant: Omnidirectionally calibrated quantization for large language models,” *arXiv preprint arXiv:2308.13137*, 2023.

[55] H. Sharma, J. Park, E. Amaro, B. Thwaites, P. Kotha, A. Gupta, J. K. Kim, A. Mishra, and H. Esmaeilzadeh, “Dnnweaver: From high-level deep network models to fpga acceleration,” in *the Workshop on Cognitive Architectures*, 2016.

[56] Y. Sheng, L. Zheng, B. Yuan, Z. Li, M. Ryabinin, B. Chen, P. Liang, C. Ré, I. Stoica, and C. Zhang, “Flexgen: High-throughput generative inference of large language models with a single gpu,” in *International Conference on Machine Learning*. PMLR, 2023, pp. 31 094–31 116.

[57] Y. Su, Y. Zhou, Q. Qiu, J. Li, Q. Xia, P. Li, X. Duan, Z. Wang, and M. Zhang, “Accurate kv cache quantization with outlier tokens tracing,” *arXiv preprint arXiv:2505.10938*, 2025.

[58] Y. Sun, R. Liu, H. Bai, H. Bao, K. Zhao, Y. Li, J. Hu, X. Yu, L. Hou, C. Yuan, X. Jiang, and W. Liu, “Flatquant: Flatness matters for llm quantization,” *arXiv preprint arXiv:2410.09426*, 2024.

[59] H. Touvron, T. Lavril, G. Izacard, X. Martinet, M.-A. Lachaux, T. Lacroix, B. Rozière, N. Goyal, E. Hambro, F. Azhar, A. Rodriguez, A. Joulin, E. Grave, and G. Lample, “Llama: Open and efficient foundation language models,” *arXiv preprint arXiv:2302.13971*, 2023.

[60] H. Touvron, L. Martin, K. Stone, P. Albert, A. Almahairi, Y. Babaei, N. Bashlykov, S. Batra, P. Bhargava, S. Bhosale, D. Bikel, L. Blecher, C. C. Ferrer, M. Chen, G. Cucurull, D. Esiobu, J. Fernandes, J. Fu, W. Fu, B. Fuller, C. Gao, V. Goswami, N. Goyal, A. Hartshorn, S. Hosseini, R. Hou, H. Inan, M. Kardas, V. Kerkez, M. Khabsa, I. Kloumann, A. Korenev, P. S. Koura, M.-A. Lachaux, T. Lavril, J. Lee, D. Liskovich, Y. Lu, Y. Mao, X. Martinet, T. Mihaylov, P. Mishra, I. Molybog, Y. Nie, A. Poulton, J. Reizenstein, R. Rungta, K. Saladi, A. Schelten, R. Silva, E. M. Smith, R. Subramanian, X. E. Tan, B. Tang, R. Taylor, A. Williams, J. X. Kuan, P. Xu, Z. Yan, I. Zarov, Y. Zhang, A. Fan, M. Kambadur, S. Narang, A. Rodriguez, R. Stojnic, S. Edunov, and T. Scialom, “Llama 2: Open foundation and fine-tuned chat models,” *arXiv preprint arXiv:2307.09288*, 2023.

[61] A. Vaswani, N. Shazeer, N. Parmar, J. Uszkoreit, L. Jones, A. N. Gomez, Ł. Kaiser, and I. Polosukhin, “Attention is all you need,” *Advances in neural information processing systems*, vol. 30, 2017.

[62] H. Wang, S. Ma, L. Dong, S. Huang, H. Wang, L. Ma, F. Yang, R. Wang, Y. Wu, and F. Wei, “Bitnet: Scaling 1-bit transformers for large language models,” *arXiv preprint arXiv:2310.11453*, 2023.

[63] G. Xiao, J. Lin, M. Seznec, H. Wu, J. Demouth, and S. Han, “Smoothquant: Accurate and efficient post-training quantization for large language models,” in *International conference on machine learning*. PMLR, 2023, pp. 38 087–38 099.

[64] G. Xiao, Y. Tian, B. Chen, S. Han, and M. Lewis, “Efficient streaming language models with attention sinks,” *arXiv preprint arXiv:2309.17453*, 2023.

[65] Z. Yao, R. Yazdani Aminabadi, M. Zhang, X. Wu, C. Li, and Y. He, “Zeroquant: Efficient and affordable post-training quantization for large-scale transformers,” *Advances in neural information processing systems*, vol. 35, pp. 27 168–27 183, 2022.

[66] Y. Yue, Z. Yuan, H. Duanmu, S. Zhou, J. Wu, and L. Nie, “Wkvquant: Quantizing weight and key/value cache for large language models gains more,” *arXiv preprint arXiv:2402.12065*, 2024.

[67] S. Q. Zhang, B. McDanel, and H. Kung, “Fast: Dnn training under variable precision block floating point with stochastic rounding,” in *2022 IEEE International Symposium on High-Performance Computer Architecture (HPCA)*. IEEE, 2022, pp. 846–860.

[68] S. Zhang, S. Roller, N. Goyal, M. Artetxe, M. Chen, S. Chen, C. Dewan, M. Diab, X. Li, X. V. Lin, T. Mihaylov, M. Ott, S. Shleifer, K. Shuster, D. Simig, P. S. Koura, A. Sridhar, T. Wang, and L. Zettlemoyer, “Opt: Open pre-trained transformer language models,” *arXiv preprint arXiv:2205.01068*, 2022.

[69] Y. Zhang, M. Wang, L. Zou, W. Liu, H.-L. Zhen, M. Yuan, and B. Yu, “Mixpe: Quantization and hardware co-design for efficient llm inference,” *arXiv preprint arXiv:2411.16158*, 2024.

[70] Y. Zhang, R. Sun, Y. Chen, T. Pfister, R. Zhang, and S. Arik, “Chain of agents: Large language models collaborating on long-context tasks,” *Advances in Neural Information Processing Systems*, vol. 37, pp. 132 208–132 237, 2024.

[71] Z. Zhang, Y. Sheng, T. Zhou, T. Chen, L. Zheng, R. Cai, Z. Song, Y. Tian, C. Ré, C. Barrett, Z. Wang, and B. Chen, “H2o: Heavy-hitter oracle for efficient generative inference of large language models,” *Advances in Neural Information Processing Systems*, vol. 36, pp. 34 661–34 710, 2023.

[72] Y. Zhao, C.-Y. Lin, K. Zhu, Z. Ye, L. Chen, S. Zheng, L. Ceze, A. Krishnamurthy, T. Chen, and B. Kasikci, “Atom: Low-bit quantization for efficient and accurate llm serving,” *Proceedings of Machine Learning and Systems*, vol. 6, pp. 196–209, 2024.

[73] Y. Zhao, D. Wu, and J. Wang, “Alisa: Accelerating large language model inference via sparsity-aware kv caching,” in *2024 ACM/IEEE 51st Annual International Symposium on Computer Architecture (ISCA)*. IEEE, 2024, pp. 1005–1017.